# Structural insights into the interaction of IL-33 with its receptors

Xi Liu[a], Michal Hammel[b], Yanfeng He[a], John A. Tainer[c,d], U-Ser Jeng[e], Linqi Zhang[f], Shuying Wang[g,h,1], and Xinquan Wang[a,1]

[a]Ministry of Education Key Laboratory of Protein Science, Center for Structural Biology, School of Life Sciences, Tsinghua University, Beijing 100084, China; [b]Physical Biosciences Division, Lawrence Berkeley National Laboratory, Berkeley, CA 94720; [c]Department of Integrative Structural and Computational Biology, Skaggs Institute of Chemical Biology, The Scripps Research Institute, La Jolla, CA 92037; [d]Life Sciences Division, Lawrence Berkeley National Laboratory, Berkeley, CA 94720; [e]National Synchrotron Radiation Research Center, Hsinchu 30076, Taiwan; [f]Comprehensive AIDS Research Center, School of Medicine, Tsinghua University, Beijing 100084, China; [g]Department of Microbiology and Immunology, National Cheng Kung University Medical College, Tainan 701, Taiwan; and [h]Center of Infectious Disease and Signaling Research, National Cheng Kung University, Tainan 701, Taiwan

Edited by K. Christopher Garcia, Stanford University, Stanford, CA, and approved August 2, 2013 (received for review May 7, 2013)

**Interleukin (IL)-33 is an important member of the IL-1 family that has pleiotropic activities in innate and adaptive immune responses in host defense and disease. It signals through its ligand-binding primary receptor ST2 and IL-1 receptor accessory protein (IL-1RAcP), both of which are members of the IL-1 receptor family. To clarify the interaction of IL-33 with its receptors, we determined the crystal structure of IL-33 in complex with the ectodomain of ST2 at a resolution of 3.27 Å. Coupled with structure-based mutagenesis and binding assay, the structural results define the molecular mechanism by which ST2 specifically recognizes IL-33. Structural comparison with other ligand–receptor complexes in the IL-1 family indicates that surface-charge complementarity is critical in determining ligand-binding specificity of IL-1 primary receptors. Combined crystallography and small-angle X-ray–scattering studies reveal that ST2 possesses hinge flexibility between the D3 domain and D1D2 module, whereas IL-1RAcP exhibits a rigid conformation in the unbound state in solution. The molecular flexibility of ST2 provides structural insights into domain-level conformational change of IL-1 primary receptors upon ligand binding, and the rigidity of IL-1RAcP explains its inability to bind ligands directly. The solution architecture of IL-33–ST2–IL-1RAcP complex from small-angle X-ray–scattering analysis resembles IL-1β–IL-1RII–IL-1RAcP and IL-1β–IL-1RI–IL-1RAcP crystal structures. The collective results confer IL-33 structure–function relationships, supporting and extending a general model for ligand–receptor assembly and activation in the IL-1 family.**

protein–protein interaction | X-ray crystallography | SAXS | cytokine signaling

Interleukin (IL)-33 has important roles in initiating a type 2 immune response during infectious, inflammatory, and allergic diseases (1–5). It was initially identified as a nuclear factor in endothelial cells and named NF-HEV (nuclear factor from high endothelial venules) (6, 7). In 2005, it was rediscovered as a new member of the IL-1 family and an extracellular ligand for the orphan IL-1 receptor family member ST2 (8). As an extracellular cytokine, IL-33 is involved in the polarization of Th2 cells and activation of mast cells, basophils, eosinophils, and natural killer cells (1–3). Recent studies also discovered that the type 2 innate lymphoid cells (ILC2s) are major target cells of IL-33 (9, 10). ILC2s express a high level of ST2 and secrete large amounts of Th2 cytokines, most notably IL-5 and IL-13, when stimulated with IL-33 (11–13). Activation of ILC2s is essential in the initiation of the type 2 immune response against helminth infection and during allergic diseases such as asthma (9, 10).

IL-33 does not have a signal peptide and is synthesized with an N-terminal propeptide upstream of the IL-1–like cytokine domain. It is preferentially and constitutively expressed in the nuclei of structural and lining cells, particularly in epithelial and endothelial cells (14, 15). Tissue damage caused by pathogen invasion or allergen exposure may lead to the release of IL-33 into extracellular environment from necrotic cells, which functions as an endogenous danger signal or alarmin (14, 16). Full-length human IL-33 consists of 270 residues and is biologically active (17, 18). It is also a substrate of serine proteases released by inflammatory cells recruited to the site of injury (18, 19). The proteases elastase, cathepsin G, and proteinase 3 cleave full-length IL-33 to release N-terminal–truncated mature forms containing the IL-1–like cytokine domain: IL-$33_{95–270}$, L-$33_{99–270}$, and IL-$33_{109–270}$ (18). These mature IL-33 forms process a 10-fold greater potency to activate ST2 than full-length IL-33 (18). Caspase-1 was also suggested to cleave IL-33 to generate an active IL-$33_{112–270}$ that is the commercially available mature IL-33 form (8). However, it was later demonstrated that this cleavage site does not exist and cleavage by caspases at other sites actually inactivates IL-33 (17, 20, 21).

The signaling of IL-33 depends on its binding to the primary receptor ST2 and subsequent recruitment of accessory receptor IL-1RAcP (8, 22, 23). The ligand-binding–induced receptor heterodimerization results in the juxtaposition of the intracellular toll/interleukin-1 receptor (TIR) domains of both receptors, which is necessary and sufficient to activate NF-κB and MAPK pathways in the target cells (24). Previously, we determined the complex structure of IL-1β with its decoy receptor

## Significance

**Interleukin (IL)-33 exerts its biological effects by binding to its specific primary receptor ST2 and the coreceptor IL-1 receptor accessory protein (IL-1RAcP). Through determining the crystal structure of IL-33 with ST2, we define the molecular basis for their specific recognition and propose that surface-charge complementarity is critical in determining ligand-binding specificity of IL-1 primary receptors. Small-angle X-ray–scattering studies also reveal that ST2 possesses significant interdomain flexibility, which is not present in the coreceptor IL-1RAcP. These molecular features are consistent with their respective roles in ligand binding and signal transduction on cell surface. Small-angle X-ray–scattering results also support and extend a detailed stepwise model for ligand–receptor assembly and activation in the IL-1 family.**

Author contributions: S.W. and X.W. designed research; X.L., M.H., Y.H., U-S.J., S.W., and X.W. performed research; X.L., M.H., J.A.T., S.W., and X.W. analyzed data; and M.H., L.Z., S.W., and X.W. wrote the paper.

The authors declare no conflict of interest.

This article is a PNAS Direct Submission.

Data deposition: The atomic coordinates and structure factors have been deposited in the Protein Data Bank, www.pdb.org (PDB ID code 4KC3).

[1]To whom correspondence may be addressed. E-mail: sswang23@mail.ncku.edu.tw or xinquanwang@mail.tsinghua.edu.cn.

This article contains supporting information online at www.pnas.org/lookup/suppl/doi:10.1073/pnas.1308651110/-/DCSupplemental.

IL-1RII and accessory receptor IL-1RAcP (25). Based on this structure and other previous studies, we proposed a general structural model for the assembly and activation of IL-1 family of cytokines with their receptors (25). In this model, ligand recognition relies on interaction of IL-1 cytokine with its primary receptor: IL-1α and IL-1β with IL-1RI; IL-33 with ST2; IL-18 with IL-18Rα; and IL-36α, IL-36β, and IL-36γ with IL-1Rrp2 (26–28). The binding forms a composite surface to recruit accessory receptor IL-1RAcP shared by IL-1α, IL-1β, IL-33, IL-36α, IL-36β, and IL-36γ and IL-18Rβ by IL-18 (26, 27). This general structural model is further supported by the subsequent structural determination of IL-1β with IL-1RI and IL-1RAcP (29). However, there are still many key missing parts in the general structural model of ligand–receptor interaction in the IL-1 family. For example, the structural basis for specific recognition of IL-33 by ST2 and IL-18 by IL-18Rα, and promiscuous recognition of IL-36α, IL-36β, and IL-36γ by IL-1Rrp2 remains elusive. The proposed general model also needs further confirmation from structural studies of other signaling complexes in the IL-1 family. To address these issues, we studied the interaction of IL-33 with its receptors by a combination of X-ray crystallography and small-angle X-ray–scattering (SAXS) methods.

## Results

**Overall Structure.** The complex structure of active IL-$33_{112–270}$ (Ser112 to Thr270) with ST2 ectodomain (Lys19 to Lys321) was determined at a resolution of 3.27 Å by the molecular replacement method (Table S1 and Fig. 1). The final model includes IL-33 residues Ser117 to Asn171, Gly179 to Val252, and Glu261 to Ser268 and ST2 residues Ser21 to Ser51, Ser56 to Lys223, Asn232 to Gly271, and Gly279 to Arg317. Three N-acetyl-D-glucosamine (NAG) glycans are linked to Asn95, Asn140, and Asn191 of ST2, respectively (Fig. 1). Other missing residues were not built because of weak electron densities. The ectodomain of ST2 consists of three IgG-like domains (D1 to D3) as expected (Fig. 1). The D1 and D2 domains pack together to form a single D1D2 module, to which the D3 domain is connected through a long linker (Fig. 1). In the complex, the ST2 wraps around IL-33 like a grasping hand with all three domains (Fig. 1).

IL-33 adopts a 12-stranded β-trefoil fold (Fig. S1). The crystal structure of IL-33 in the complex superimposes well with solution structure of IL-33 determined by NMR method with an r.m.s.d. of 1.2 Å for 123 matched Cα atoms (30). Twelve β-strands forming the β-trefoil fold are conserved in both structures, whereas conformational variations reside in the loops connecting the strands, especially in loops β2-β3, β3-β4, β4-β5, β10-β11, and β11-β12 involved in receptor interaction (Fig. S1). The β4-β5 and β11-β12 loops are disordered in the crystal structure, and in the NMR structure, the β4-β5 loop is also the region with the most diverse conformation (Fig. S1). These two loops are involved in the recruitment of accessory receptor IL-1RAcP after the binding of IL-33 with ST2, and their roles are discussed below.

All members except SIGIRR in the IL-1 receptor family have three Ig-like domains (D1 to D3) in the extracellular region (26). The packing and orientation between D1 and D2 domains in the D1D2 module are conserved among primary receptors ST2, IL-1RI, and IL-1RII, the structures of which have been determined (Fig. S2) (25, 29, 31, 32). The linker connecting the D3 domain to the D1D2 module is flexible, resulting in different orientations of the D3 domain among these three primary receptors when they bind their respective ligands (Fig. S2).

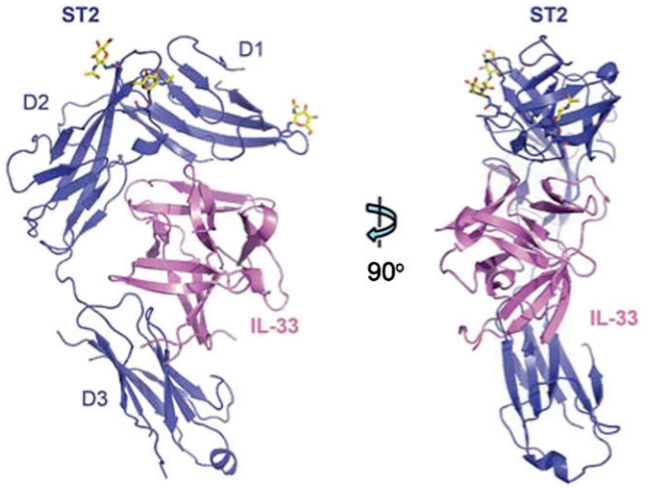


**Fig. 1.** Crystal structure of IL-33 in complex with ST2 receptor. IL-33 and ST2 are colored with purple and blue, respectively, and N-linked glycans in ST2 are presented as "sticks" with yellow color.

**IL-33/ST2 Interface and Binding Assay.** IL-33 interacts with all three domains of ST2, and a large surface area of ∼1,798 $Å^2$ on IL-33 and ∼1,785 $Å^2$ on ST2 are buried upon binding. This large binding interface is composed of two separate binding sites (Fig. 2). At site 1, thirteen IL-33 residues, from β3-strand, β1-β2, β2-β3, β3-β4, and β10-β11 loops, have contacts with the D1D2 module of ST2 receptor (Fig. S3). Among these residues, Glu144, Glu148, Asp149, and Asp244 form salt-bridge interactions with ST2 residues Arg38, Lys22, Arg198, and Arg35, respectively (Fig. 2). Glu144 and Asp149 also form hydrogen-bonding interactions with ST2 receptor main-chain atoms (Fig. 2). At site 2, eight IL-33 residues from β1-, β4-, β5-strands and β8-β9 loop have contacts with the D3 domain of ST2 (Fig. S3). The chemical nature here is a mixture of hydrophobic and hydrophilic interactions. Among the IL-33–interacting residues, four of them are hydrophobic and a significant hydrophobic cluster is formed by IL-33 residues Tyr164 and Leu182 and ST2 residues Leu246, Leu306, and Leu311 (Fig. 2). Acidic residue Glu165 has salt-bridge interaction with Arg313 of ST2 (Fig. 2).

Previous efforts to identify "hot spot" residues of IL-33 for ST2 interaction were based on NMR chemical-shift perturbation data and subsequent mutagenesis and affinity measurements (30). Twenty-eight IL-33 mutants were examined, and only one mutant (E144K) had a pronounced effect on the interaction between IL-33 and ST2 by decreasing the affinity sevenfold from 0.45 to 3.15 nM (30). We measured the ST2-binding affinities of IL-33 mutants identified by structural analysis of the IL-33/ST2 interface with surface plasmon resonance (SPR) method (Table S2). These mutation sites were not examined in the previous report except the Glu144 position. In our measurements, wild-type IL-33 bound to ST2 ectodomain with an affinity of 0.74 nM (Table S2 and Fig. S4), comparable to the previously reported 0.45 nM (30). All IL-33 mutations of acidic residues at site I (E144K, E148K, D149K, and D244K) decreased the ST2-binding affinity. E144K and D244K mutants exhibited ∼two- to threefold reduction from 0.74 to 1.89 and 1.65 nM, respectively (Table S2 and Fig. S4). Mutation E148K had a more pronounced effect on the binding with ∼sevenfold affinity reduction from 0.74 to 5.15 nM (Table S2 and Fig. S4). Mutation at Asp149 position (D149K) reduced the binding of IL-33 with ST2 to an undetectable level by SPR method (Table S2 and Fig. S4). At site 2, mutation of acidic residue Glu165 (E165K) also decreased the binding affinity ∼eightfold from 0.74 to 6.07 nM, whereas mutations of hydrophobic residues Tyr163 and Leu182 had less effect on the binding (Table S2 and Fig. S4).

**Comparison of Binding Site 1 in Different Ligand–Receptor Complexes.** Previous crystal structures revealing ligand recognition by primary receptor are only available for IL-1β–IL-1RI, IL-1β–IL-1RII, and IL-1Ra–IL-1RI pairs (25, 29, 31, 32). Structural comparison of

BIOCHEMISTRY

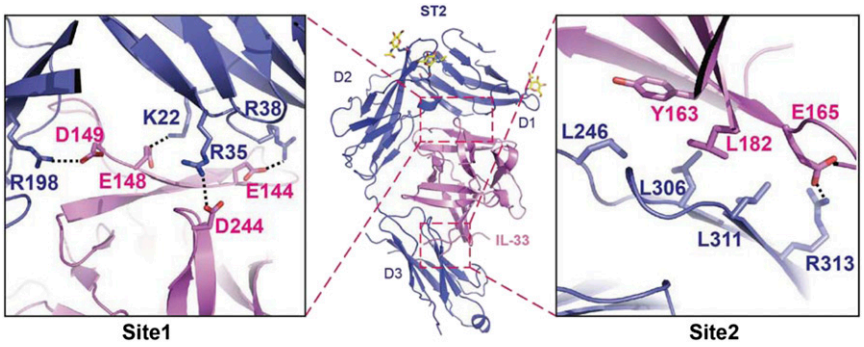


**Fig. 2.** IL-33/ST2 interface. There are two distinct binding sites between IL-33 and ST2. At site 1, IL-33 acidic residues Glu144, Glu148, Asp149, and Asp244 form salt-bridge interactions with ST2 basic residues Arg38, Lys22, Arg198, and Arg35, respectively. Glu144 and Asp149 of IL-33 also have hydrogen-bonding interactions with ST2 main chain atoms. At site 2, IL-33 acidic residue Glu165 has salt-bridge interaction with Arg313 of ST2. A significant hydrophobic cluster at site 2 involves residues Tyr163 and Leu182 of IL-33 and Leu246, Leu306, and Leu311 of ST2.

IL-33–ST2 with them revealed a similar architecture with the involvement of all three Ig-like domains (D1 to D3) and two separate sites in ligand binding (Fig. 3*A*). Site 1 is more structurally conserved than site 2 in different ligand–receptor pairs because of rigidity of the D1D2 module in different receptors. However, a more close examination revealed differences of IL-33 from IL-1β and IL-1Ra in receptor binding at site 1. We have shown that IL-33 acidic residues Glu144, Glu148, Asp149, and Asp244 form salt-bridge interactions with side chains of basic residues of ST2 receptor (Fig. 2), which is also evidenced by the complementary electrostatic potential on the surfaces of IL-33 and ST2 at site 1 (Fig. 3*B*). The surface of IL-33 at site 1 exhibits strong negative charge, and the corresponding surface of ST2 is dominated by positive charge (Fig. 3*B*). In contrast, IL-1β–critical residues Arg21, Gln15, and Gln32 at site 1 interact with IL-1RI and IL-1RII mainly through van der Waals contacts and hydrogen bonds with receptor main-chain atoms (25, 29, 31). This phenomenon has also been observed at the binding site 1 between IL-1Ra and IL-1RI (32). Surface electrostatic-potential analyses also showed that the surfaces of IL-1β and IL-1Ra at site 1 are not dominated by negative charge, and the corresponding surfaces of IL-1RI and IL-1RII have no remarkable electrostatic properties (Fig. 3*C*). Although the crystal structure of IL-18 in complex with IL-18Rα is not available, IL-18 has an obvious patch with negative charge at potential binding site 1 (Fig. 3*D*) (33, 34), similar to that of IL-33.

**Solution X-Ray–Scattering Studies of Receptors and Ligand–Receptor Complexes.** Currently, all available structures of the IL-1 primary receptors are in ligand-bound state and have flexibly linked

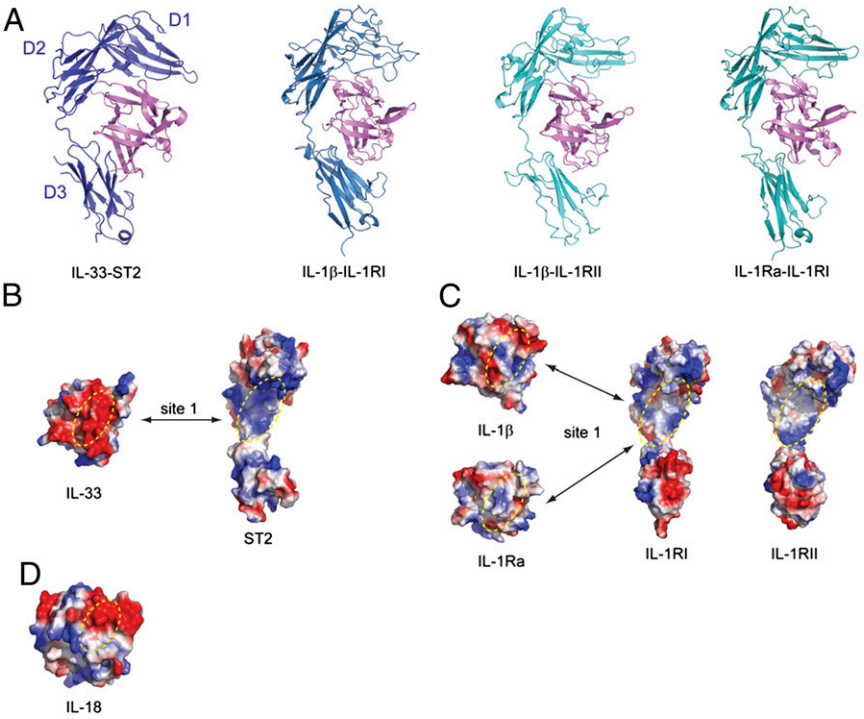


**Fig. 3.** Surface electrostatic-potential analyses of binding site 1. (*A*) Crystal structures of IL-33–ST2, IL-1β–IL-1RI, IL-1β–IL-1RII, and IL-1Ra–IL-1RI pairs after alignment based on the bound ligand. (*B*) IL-33 and ST2 have charge complementarity at binding site 1 (yellow dotted circle), with the IL-33 surface negatively charged (red) and the ST2 surface positively charged (blue). (*C*) There is no obvious charge complementarity at binding site 1 of IL-1β/IL-1RI, IL-1β/IL-1RII, and IL-1Ra/IL-1RI interfaces. (*D*) IL-18 has a negatively charged patch on the surface of potential binding site 1.

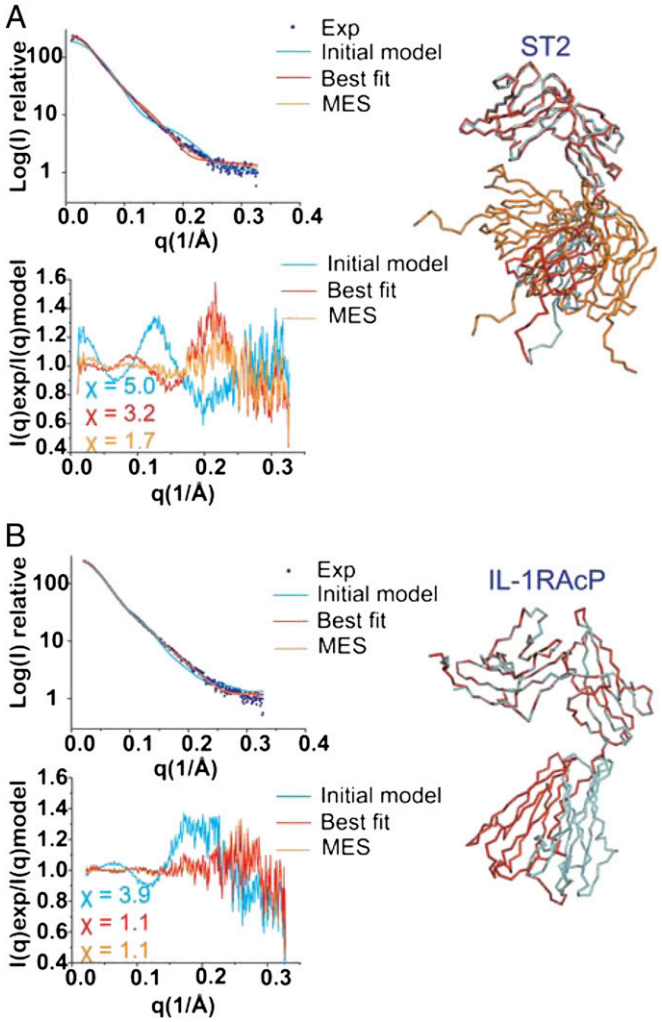


**Fig. 4.** Flexibility of ST2 (*A*) and rigidity of IL-1RAcP (*B*) in solution. Comparison of experimental data and calculated scattering profiles for ST2 (*A*) and IL-1RAcP (*B*). Experimental data are represented in blue dots. Cyan, red, and light orange lines represent the theoretical scattering curves of the initial model derived from crystal structure (cyan), the single best-fit conformation (red), and the assembly from MES (light orange). Residuals calculated as $I(q)_{experimental}/I(q)_{model}$ are shown below the scattering curves.

domains. However, the degree of flexibility between domains of the receptors correlated with their dynamic nature relevant to molecular recognition has not been investigated. Using a combination of crystallography and SAXS (35), we characterized the functional conformations of the receptors in solution and revealed conformational changes upon complex formation with the ligand. ST2 and IL-1RAcP SAXS data were collected (Fig. S5) and further analyzed to determine whether the receptors exist as well-defined conformations or as an assembly of different conformers in solution by using the program BILBOMD (36), in which the D1D2 module and D3 domain were treated as two separate rigid bodies connected by a flexible linker. In BILBOMD, 10,000 distinct conformers were generated by constrained molecular dynamics (MD) simulation, theoretical scattering profiles were calculated by FoXS (37), and then Minimal Ensemble Search (MES) were applied to select a subset containing one to four conformers that best fit the experimental data (36). The full-atomic model is crucial to match the experimental data (38); therefore, missing loops and residues in ST2 and IL-1RAcP ligand-bound crystal structures were constructed with MODELLER (39). For ST2, the theoretically calculated SAXS profile from initial model does not agree well with experimental data ($\chi = 5.0$) (Fig. 4*A*). An ensemble of three conformers fits the data significantly much better ($\chi = 1.7$) than the single best-fit conformer ($\chi = 3.2$) (Fig. 4*A*). For IL-1RAcP, the single best-fit model with a small movement in D3 domain compared with crystal structure improves the fit ($\chi = 1.1$) than the initial full-atomic model derived from crystal structure ($\chi = 3.9$), and MES approach does not improve the fit ($\chi = 1.1$) (Fig. 4*B*).

The crystal structure of IL-33–ST2–IL-1RAcP complex is still not available. To resolve its molecular architecture, we generated a model of IL-33–ST2–IL-1RAcP by fitting IL-33–ST2 crystal structure into the previously determined IL-1β–IL-1RII–IL-1RAcP ternary complex and replacing IL-1β and IL-1RII with IL-33 and ST2, respectively. To validate this model and to compare the receptors in ligand-bound and ligand-unbound state, we collected the SAXS data on IL-33–ST2 and IL-33–ST2–IL-1RAcP complexes (Fig. S5). Theoretical SAXS profiles from initial full-atomic models of IL-33–ST2 and IL-33–ST2–IL1RAcP complexes fit the experimental data well, with the $\chi$ value of 1.5 and 1.8, respectively (Fig. 5 *A* and *B*).

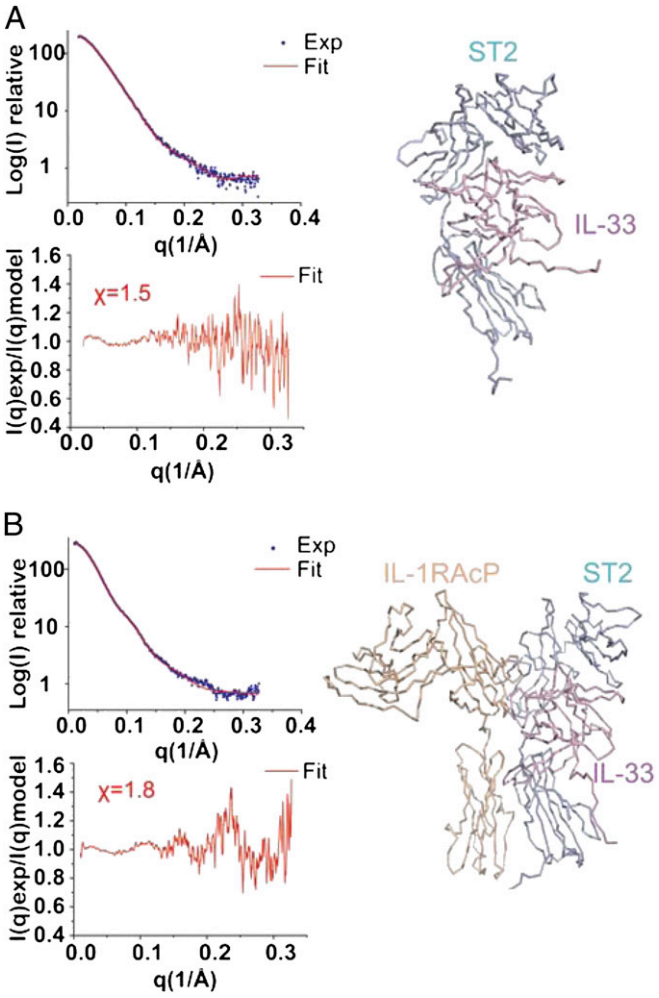


**Fig. 5.** Solution architecture of IL-33–ST2 (*A*) and IL-33–ST2–IL-1RAcP (*B*) complexes. Good fit of the experimental data (blue dot) and the full-atomic models derived from crystal structures (red line). Residuals calculated as $I(q)_{experimental}/I(q)_{model}$ are shown below the scattering curves.

## Discussion

The IL-1 family consists of eleven members, so it is important to examine conserved and variable structural features relevant to a general understanding of their interactions with receptors and activities. In the present study, we determined the crystal structure of IL-33 in complex with the ectodomain of its primary receptor ST2 (Fig. 1 and Table S1) and delineated the solution conformational states of ST2 and accessory receptor IL-1RAcP (Fig. 4), which illuminate the structural basis of how the specific IL-33–receptor complex drives biological processes and how the level of flexibility within receptors is relevant to molecular recognition. Structural comparison with IL-1β–IL-1RI, IL-1β–IL-1RII, and IL-1Ra–IL-1RI pairs showed that all ligand-binding IL-1 primary receptors recognize their respective ligands in a similar way (Fig. 3*A*) (25, 29, 31, 32). However, ST2-receptor specifically recognizes IL-33, whereas IL-1RI and IL-1RII promiscuously recognize IL-1α, IL-1β, and IL-1Ra, which share a similar β-trefoil fold but with low sequence homologies. Our structure-based mutagenesis and binding assay identified IL-33 acidic residues Glu148 and Asp149 at site 1 and Glu165 at site 2, important for high-affinity binding with ST2 receptor (Fig. 2 and Table S2), and these residues form specific salt-bridge interactions with basic residues of ST2 receptor. Surface electrostatic-potential analysis also revealed obvious charge complementarity at site 1 of the IL-33/ST2 binding interface (Fig. 3*B*). In contrast, there is no obvious charge complementarity at the binding interfaces of IL-1RI and IL-1RII in complex with IL-1β and IL-1Ra (Fig. 3*C*). IL-18 is another member in the IL-1 family that has its own specific primary receptor, IL-18Rα, and it has a negative charge patch at the surface of binding site 1 (Fig. 3*D*). Therefore, we propose that charge complementarity may play important roles in the specific recognition of IL-18 by IL-18Rα. We further suggest that ST2 and IL-18Rα mainly use charge complementarity at site 1 to achieve ligand-binding specificity, whereas IL-1RI, IL-1RII, and IL-1Rrp2 avoid them to achieve ligand-binding promiscuity.

SAXS studies also revealed that ST2 has naturally built-in flexibility between the D3 domain and D1D2 module. MES-based search selected a subset of three major conformers of ST2 ectodomain, which can be regarded as open, half-open, and closed states considering the orientation of the D3 domain with respect to the D1D2 module (Fig. S6*A*). The ST2 half-open conformer resembles the conformation of ST2 after binding to IL-33 (Fig. S6*B*), and the ST2 closed conformer resembles the conformation of IL-1RI when it binds to a peptide antagonist (40) (Fig. S6*B*). Although IL-1RI has not been structurally studied in solution, in the complex, IL-1RI is able to adopt at least two conformations: one is the closed state in complex with the peptide antagonist (40), and the other is the half-open conformation in complex with its cytokine ligands IL-1β or IL-1Ra (31, 32). Together, these results suggest that primary receptors in the IL-1 family are flexible between the D3 domain and D1D2 module, which enables the D3 domain to bind their respective ligands from the bottom side at site 2. After binding, the IL-33–ST2 complex forms a rigid conformation, evidenced by the excellent match of one single conformer with the experimental SAXS data (Fig. 5*A*). This rigid binary complex then provides a molecular platform for the recruitment of accessory receptor IL-1RAcP.

Our SAXS studies revealed that IL-1RAcP has a preference for a single conformation in solution (Fig. 4*B*), indicating that IL-1RAcP is not as flexible as ST2 between the D3 domain and D1D2 module. IL-1RAcP conformer in solution is even more closed between the D3 domain and D1D2 module compared with its crystal structure in ligand-bound state (Fig. 4*B*) (25, 29). The previously determined crystal structure has implied that IL-1RAcP is rigid because the linker is not extended and has interactions with the D1D2 module and D3 domain (25). However, that structure captures the state of IL-1RAcP in the ternary complex. Here, we have found a similarly rigid conformation of unbound IL-1RAcP in solution by SAXS study, and this supports our previous hypothesis that steric hindrance contributes to the inability of IL-1RAcP to directly engage cytokines.

A prior SAXS study proposed an IL-33–ST2–IL-1RAcP model that is different from the determined IL-1β–IL-1RII–IL-1RAcP and IL-1β–IL-1RI–IL-1RAcP crystal structures (30). With determined IL-33–ST2 and IL-1RAcP crystal structures, we are able to interpret SAXS data in a more accurate way (41). The IL-33–ST2–IL-1RAcP ternary complex model derived from IL-1β–IL-1RII–IL-1RAcP structure fitted the experimental SAXS data well (Fig. 5*B*), consistent with the "LEFT" architecture of the IL-1 signaling complex (25, 29). In the IL-1β–IL-1RII–IL-1RAcP and IL-1β–IL-1RI–IL-1RAcP structures (25, 29), IL-1β β4-β5 and β11-β12 loops are involved in the interaction with IL-1RAcP. These two loops are disordered in the IL-33–ST2 complex structure, and they are expected to adopt suitable conformations to contact with IL-1RAcP. IL-1RAcP is a shared cytokine receptor like common γ-chain and gp130 (42), but the structural basis for its promiscuous binding by distinct ligand–primary receptor complexes is still not well understood. The β4-β5 and β11-β12 loops binding to IL-1RAcP have low sequence homology among different agonists (IL-1α, IL-1β, IL-33, IL-36α, IL-36β, and IL-36γ). The D2 and D3 domains also have low sequence homology among different primary receptors including IL-1RI, IL-1RII, ST2, and IL-1Rrp2. However, interactions shared by IL-1RI and IL-1RII to bind IL-1RAcP are found in a small hydrophobic patch, which is formed by Ile135, Leu180, and Ile181 in IL-1RAcP and Val160 (Val173 in IL-1RII) and Ile165 (Leu180 in IL-1RII) in IL-1RI (29). ST2 has His162 and Val167 in these two positions, respectively, and there is another hydrophobic residue Phe165 nearby (Fig. S7). Therefore, among many disparate molecular interactions, this conserved hydrophobic patch may play important roles in the binding of IL-1RAcP by different ligand–primary receptor complexes. The cross-reactivity of IL-1RAcP would be better understood by future crystal structural studies of other signaling complexes involving IL-1RAcP in the IL-1 family.

Our results support a more detailed stepwise assembly and activation model of the IL-33 signaling complex (Fig. S8). The ectodomain of ST2 adopts different conformation before IL-33 binding because of flexibility between the D3 domain and D1D2 module. The concave electropositive surface at binding site 1 specifically recognizes the electronegative surface of IL-33, initiating the specific recognition of IL-33. The D3 domain of ST2 adopts a final best position to cover the bound IL-33 from the bottom side at binding site 2, helping form a very stable IL-33–ST2 binary complex with a rigid conformation. The IL-33–ST2 complex then recruits accessory receptor IL-1RAcP, contributed to by both IL-33 and ST2. The final assembly of the ternary complex juxtaposes the intracellular TIR domains of ST2 and IL-1RAcP receptors, which triggers the subsequent intracellular signaling pathways. This stepwise binding model and built-in flexibility of ligand-binding primary receptors may be general to other members of the IL-1 family.

## Materials and Methods

Plasmid DNA constructions, protein expression and purification, crystallization and diffraction data collection, structural determination and refinement, and surface plasmon resonance analysis are described in detail in *SI Materials and Methods*. SAXS data were collected at the Advanced Light Source beamline 12.3.1 (structurally integrated biology for life sciences), Lawrence Berkeley National Laboratory as described (43, 44). SAXS data analysis and modeling are described in *SI Materials and Methods*.

**ACKNOWLEDGMENTS.** We thank J. H. He and S. Huang (beamline BL17U of Shanghai Synchrotron Research Facility) for assistance with data collection

and J. W. Wang and H. P. Gong for assistance with structural determination. This work was supported by Ministry of Science and Technology Grants 2010CB912402 and 2011CB910502 (to X.W.), the Tsinghua University Initiative Scientific Program (X.W.), National Science Council Grant 98-2311-B-006-004-MY3 (to S.W.), the Integrated Diffraction Analysis Technologies Program under the contract number DE-AC02-05CH11231 of the Department of Energy (to M.H. and J.A.T.), and National Institutes of Health Grant GM105404 (to M.H. and J.A.T.).

1. Liew FY, Pitman NI, McInnes IB (2010) Disease-associated functions of IL-33: The new kid in the IL-1 family. *Nat Rev Immunol* 10(2):103–110.
2. Oboki K, Ohno T, Kajiwara N, Saito H, Nakae S (2010) IL-33 and IL-33 receptors in host defense and diseases. *Allergol Int* 59(2):143–160.
3. Smith DE (2010) IL-33: A tissue derived cytokine pathway involved in allergic inflammation and asthma. *Clin Exp Allergy* 40(2):200–208.
4. Palmer G, Gabay C (2011) Interleukin-33 biology with potential insights into human diseases. *Nat Rev Rheumatol* 7(6):321–329.
5. Milovanovic M, et al. (2012) IL-33/ST2 axis in inflammation and immunopathology. *Immunol Res* 52(1-2):89–99.
6. Onda H, et al. (1999) Identification of genes differentially expressed in canine vasospastic cerebral arteries after subarachnoid hemorrhage. *J Cereb Blood Flow Metab* 19(11):1279–1288.
7. Baekkevold ES, et al. (2003) Molecular characterization of NF-HEV, a nuclear factor preferentially expressed in human high endothelial venules. *Am J Pathol* 163(1): 69–79.
8. Schmitz J, et al. (2005) IL-33, an interleukin-1-like cytokine that signals via the IL-1 receptor-related protein ST2 and induces T helper type 2-associated cytokines. *Immunity* 23(5):479–490.
9. Spits H, Cupedo T (2012) Innate lymphoid cells: Emerging insights in development, lineage relationships, and function. *Annu Rev Immunol* 30:647–675.
10. Scanlon ST, McKenzie AN (2012) Type 2 innate lymphoid cells: New players in asthma and allergy. *Curr Opin Immunol* 24(6):707–712.
11. Neill DR, et al. (2010) Nuocytes represent a new innate effector leukocyte that mediates type-2 immunity. *Nature* 464(7293):1367–1370.
12. Moro K, et al. (2010) Innate production of T(H)2 cytokines by adipose tissue-associated c-Kit(+)Sca-1(+) lymphoid cells. *Nature* 463(7280):540–544.
13. Price AE, et al. (2010) Systemically dispersed innate IL-13-expressing cells in type 2 immunity. *Proc Natl Acad Sci USA* 107(25):11489–11494.
14. Moussion C, Ortega N, Girard JP (2008) The IL-1-like cytokine IL-33 is constitutively expressed in the nucleus of endothelial cells and epithelial cells in vivo: A novel 'alarmin'? *PLoS ONE* 3(10):e3331.
15. Küchler AM, et al. (2008) Nuclear interleukin-33 is generally expressed in resting endothelium but rapidly lost upon angiogenic or proinflammatory activation. *Am J Pathol* 173(4):1229–1242.
16. Haraldsen G, Balogh J, Pollheimer J, Sponheim J, Küchler AM (2009) Interleukin-33 - cytokine of dual function or novel alarmin? *Trends Immunol* 30(5):227–233.
17. Cayrol C, Girard JP (2009) The IL-1-like cytokine IL-33 is inactivated after maturation by caspase-1. *Proc Natl Acad Sci USA* 106(22):9021–9026.
18. Lefrançais E, et al. (2012) IL-33 is processed into mature bioactive forms by neutrophil elastase and cathepsin G. *Proc Natl Acad Sci USA* 109(5):1673–1678.
19. Bae S, et al. (2012) Contradictory functions (activation/termination) of neutrophil proteinase 3 enzyme (PR3) in interleukin-33 biological activity. *J Biol Chem* 287(11): 8205–8213.
20. Lüthi AU, et al. (2009) Suppression of interleukin-33 bioactivity through proteolysis by apoptotic caspases. *Immunity* 31(1):84–98.
21. Talabot-Ayer D, Lamacchia C, Gabay C, Palmer G (2009) Interleukin-33 is biologically active independently of caspase-1 cleavage. *J Biol Chem* 284(29):19420–19426.
22. Ali S, et al. (2007) IL-1 receptor accessory protein is essential for IL-33-induced activation of T lymphocytes and mast cells. *Proc Natl Acad Sci USA* 104(47):18660–18665.
23. Chackerian AA, et al. (2007) IL-1 receptor accessory protein and ST2 comprise the IL-33 receptor complex. *J Immunol* 179(4):2551–2555.
24. Dunne A, O'Neill LA (2003) The interleukin-1 receptor/Toll-like receptor superfamily: Signal transduction during inflammation and host defense. *Sci STKE* 2003(171):re3.
25. Wang D, et al. (2010) Structural insights into the assembly and activation of IL-1β with its receptors. *Nat Immunol* 11(10):905–911.
26. Dinarello CA (2009) Immunological and inflammatory functions of the interleukin-1 family. *Annu Rev Immunol* 27:519–550.
27. Sims JE, Smith DE (2010) The IL-1 family: Regulators of immunity. *Nat Rev Immunol* 10(2):89–102.
28. Dinarello C, et al. (2010) IL-1 family nomenclature. *Nat Immunol* 11(11):973.
29. Thomas C, Bazan JF, Garcia KC (2012) Structure of the activating IL-1 receptor signaling complex. *Nat Struct Mol Biol* 19(4):455–457.
30. Lingel A, et al. (2009) Structure of IL-33 and its interaction with the ST2 and IL-1RAcP receptors—insight into heterotrimeric IL-1 signaling complexes. *Structure* 17(10): 1398–1410.
31. Vigers GP, Anderson LJ, Caffes P, Brandhuber BJ (1997) Crystal structure of the type-I interleukin-1 receptor complexed with interleukin-1beta. *Nature* 386(6621):190–194.
32. Schreuder H, et al. (1997) A new cytokine-receptor binding mode revealed by the crystal structure of the IL-1 receptor with an antagonist. *Nature* 386(6621):194–200.
33. Kato Z, et al. (2003) The structure and binding mode of interleukin-18. *Nat Struct Biol* 10(11):966–971.
34. Kim SH, et al. (2002) Identification of amino acid residues critical for biological activity in human interleukin-18. *J Biol Chem* 277(13):10998–11003.
35. Putnam CD, Hammel M, Hura GL, Tainer JA (2007) X-ray solution scattering (SAXS) combined with crystallography and computation: Defining accurate macromolecular structures, conformations and assemblies in solution. *Q Rev Biophys* 40(3):191–285.
36. Pelikan M, Hura GL, Hammel M (2009) Structure and flexibility within proteins as identified through small angle X-ray scattering. *Gen Physiol Biophys* 28(2):174–189.
37. Schneidman-Duhovny D, Hammel M, Sali A (2010) FoXS: A web server for rapid computation and fitting of SAXS profiles. *Nucleic Acids Res* 38(Web Server issue): W540–W544.
38. Hammel M (2012) Validation of macromolecular flexibility in solution by small-angle X-ray scattering (SAXS). *Eur Biophys J* 41(10):789–799.
39. Yang Z, et al. (2012) UCSF Chimera, MODELLER, and IMP: An integrated modeling system. *J Struct Biol* 179(3):269–278.
40. Vigers GP, Dripps DJ, Edwards CK, 3rd, Brandhuber BJ (2000) X-ray crystal structure of a small antagonist peptide bound to interleukin-1 receptor type 1. *J Biol Chem* 275(47):36927–36933.
41. Rambo RP, Tainer JA (2013) Accurate assessment of mass, models and resolution by small-angle scattering. *Nature* 496(7446):477–481.
42. Wang X, Lupardus P, Laporte SL, Garcia KC (2009) Structural biology of shared cytokine receptors. *Annu Rev Immunol* 27:29–60.
43. Hura GL, et al. (2009) Robust, high-throughput solution structural analyses by small angle X-ray scattering (SAXS). *Nat Methods* 6(8):606–612.
44. Classen S, et al. (2013) Implementation and performance of SIBYLS: A dual endstation small-angle X-ray scattering and macromolecular crystallography beamline at the Advanced Light Source. *J Appl Cryst* 46(Pt 1):1–13.

# Supporting Information

## Liu et al. 10.1073/pnas.1308651110

### SI Materials and Methods

**Protein Expression and Purification.** IL-$33_{112–270}$ was cloned into vector pGEX-6P-1 and expressed as a fusion protein with N-terminal GST tag. The fusion protein was expressed in *Escherichia coli* BL21 (DE3) that was induced with 0.6 mM isopropyl-β-D-thiogalactopyranoside at 0.6–0.8 $OD_{600}$ in overnight cultures grown at 290 K. The cells were harvested by centrifugation at 3,725 × *g* for 15 min and suspended with lysis buffer containing 10 mM Hepes (pH 7.2), 150 mM NaCl, and 2 mM DTT. After sonication, the lysate was centrifuged at 23,000 × *g* for 1 h, and the supernatant containing GST–IL-$33_{112–270}$ was transferred to a Glutathione Sepharose 4B column. After extensive wash of the column with lysis buffer, the bound fusion protein was digested on column with 3C PreScission protease. The released IL-$33_{112–270}$ without GST tag was collected and further purified by gel-filtration chromatography using the Superdex 200 High Performance column (GE Healthcare) with running buffer containing 10 mM Hepes (pH 7.2) and 150 mM NaCl. All mutants of IL-$33_{112–270}$ were expressed and purified in the same way.

The extracellular domain of ST2 (ST2-ECD) (residues Lys19 to Lys321) was expressed using the Bac-to-Bac baculovirus expression system (Invitrogen). *Spodoptera frugiperda* Sf9 insect cells were maintained in Insect-Xpress protein-free medium (Lonza) without serum. The ST2-ECD with an N-terminal gp67 signal peptide to facilitate secretion and a C-terminal $His_6$ tag was cloned into the pFastBac Dual vector (Invitrogen). The construct was transformed into bacterial DH10Bac competent cells, and the extracted bacmid was then transfected into Sf9 cells in the presence of Cellfectin II Reagent (Invitrogen). The low-titer viruses were harvested after incubation of the transfected cells at 300 K for 7 d and were then amplified for two more rounds. The amplified high-titer viruses were used to infect 4 L of Sf9 cells at a density of $2 \times 10^6$ cells per milliliter. The supernatant of cell culture containing ST2-ECD was harvested 60 h after infection and concentrated and buffer-exchanged to HBS [10 mM Hepes (pH 7.2) and 150 mM NaCl]. ST2-ECD was captured by nickel-charged resin (GE Healthcare) and eluted with 300 mM imidazole in HBS buffer (pH 7.2) and then further purified by gel-filtration chromatography using the Superdex 200 High Performance column (GE Healthcare). The extracellular domain of IL-1RAcP (IL-1RAcP-ECD) was expressed and purified in the same way.

Purified IL-$33_{112–270}$ and ST2-ECD were mixed, left on ice for 1 h, and purified by gel-filtration chromatography using the Superdex 200 High Performance column (GE Healthcare) to obtain the IL-33–ST2 complex. The binary complex was mixed with IL-1RAcP-ECD and then purified by gel-filtration chromatography to obtain the IL-33–ST2–IL-1RAcP ternary complex.

**Crystallization and Data Collection.** The crystals of the IL-33–ST2 complex were grown at 291 K by vapor diffusion in hanging drops composed of equal volumes of protein solution [16 mg/mL in 10 mM Hepes (pH 7.2) and 150 mM NaCl] and reservoir solution [100 mM sodium malonate (pH 4.5), 12% (wt/vol) PEG3350, 6% (vol/vol) 2-Methyl-2,4-pentanediol (MPD), and 0.007% (wt/vol) mellitic acid]. Selenomethionine-labeled crystals were grown with the same condition. All crystals were cryoprotected by soaking in well solution supplemented with 30% (vol/vol) glycerol for 10 s and then flash-cooled to 100 K in liquid nitrogen. All datasets were collected on beamline BL17U at the Shanghai Synchrotron Research Facility (SSRF) and processed with HKL2000 (1).

**Structure Determination and Refinement.** A molecular replacement solution of IL-$33_{112–270}$ was determined with the program PHASER (2) using the published IL-33 NMR solution structure [Protein Data Bank (PDB) ID code 2KLL] as the search model. The positions of the D1D2 module and D3 domain of ST2 were also determined separately with the program PHASER using the D1D2 module and D3 domain of IL-1RI (PDB ID code 1IRA) as search models. Iterative refinement with the program PHENIX (3) and model building with the program COOT (4) using the B-factor–sharpened electron-density map were conducted, yielding a final model with $R_{work}$ of 23.8% and $R_{free}$ of 28.7%. The quality of the model was validated with the program PROCHECK (5), and all structure figures were made with the program PYMOL (6).

**Surface Plasmon Resonance Analysis.** Real-time binding and the following analyses by surface plasmon resonance (SPR) were carried out on a BIAcore T200 instrument (GE Healthcare) at 298 K. ST2-ECD was immobilized on a research-grade CM5 sensor chip by the amine-coupling method. Flow cell 1 was left blank as a reference. ST2-ECD (10 μg/mL) in sodium acetate buffer (10 mM; pH 5.0) was immobilized to 1,000–1,200 response units on the flow cell, and the surface was then blocked with an injection of 1 M ethanolamine (pH 8.0) for 7 min. An injection of 10 mM NaOH for 10 s was carried out to remove noncovalently bound ST2-ECD. For the collection of data for kinetic analysis, IL-$33_{112–270}$ and its mutants in a buffer of 10 mM Hepes (pH 7.2), 150 mM NaCl, and 0.005% (vol/vol) Tween-20 were injected over the flow cells at various concentrations at a 30 μL/min flow rate. The IL-33–ST2 complex was allowed to associate for 60 s and dissociate for 240 s. Data were analyzed with the BIAcore T200 evaluation software by fitting to a 1:1 Langmuir binding fitting model.

**Small-Angle X-Ray–Scattering Data Collection and Analysis.** Data were collected at beamline 23A, National Synchrotron Radiation Research Center (NSRRC) and at beamline 12.3.1 (SIBYLS, structurally integrated biology for life sciences), Advanced Light Source, Lawrence Berkeley National Laboratory. A series of scattering curves were collected with various concentration of protein samples ranged 0.5–5 mg/mL. At the NSRRC 23A beamline, 100 μL of proteins in a sample cell was exposed for 30 and 60 s, and data were collected at wavelength λ = 0.8857 Å (energy, 14.000 KeV) with sample-to-detector distance 2.5 m, resulting in $q$ ranging from 0.0085 to 0.37 $Å^{-1}$ (7). The scattering vector $q$ is defined as $q = 4\pi \sin\theta/\lambda$, where 2θ is the scattering angle. At the SIBYLS beamline, proteins were subjected to size-exclusion chromatography before data collection; 25 μL of samples was taken from the column fractions and transferred to a 96-well plate, without further concentrating the samples to avoid aggregation. Proteins were loaded into the sample cell by pipetting robot platform (8) and then exposed for 0.5, 1, and 4 s at wavelength λ = 1.0 Å, with sample-to-detector distance 1.5 m, corresponding to $q$ ranging from 0.001 to 0.32 $Å^{-1}$. All experiments were performed at 20 °C. Corresponding to each protein sample, data were collected on a buffer sample under identical experimental conditions, and beamline-specific software was used for subtracting buffer signal from protein signal (8). Following data reduction, data were analyzed with the SCATTER. Scattering curves collected at different concentrations were analyzed separately; the radius of gyration $R_g$ values were computed from Guinier plots (9) for investigating aggregation. Subsequently, curves measured at different protein

concentrations were merged using our program SCATTER. Pair distribution function P(r) was computed using the program GNOME (10).

**Small-Angle X-Ray–Scattering Modeling.** The full-atomic models were built with the program MODELLER (11) to construct the missing loops and linkers in crystal structures. These models were used as templates for rigid-body modeling in the program BILBOMD (12), which applies the molecular dynamics (MD) stimulations to explore conformational space of the flexible domains. In the BILBOMD strategy, the theoretical small-angle X-ray–scattering (SAXS) profile for each registered conformation and the corresponding fit to the experimental data were calculated using the program FoXS (13). Minimal Ensemble Search was performed to select appropriate ensemble from pool of ~10,000 MD-generated conformations to validate macromolecular flexibility. The best ensemble was calculated to best fit the experimental curve I(q) experiment minimizing the discrepancy $\chi$ between the experimental and calculated multiconformational profile. The multiconformational scattering I(q) from such a minimal ensemble is computed by averaging and weighting the individual scattering profiles from the conforms.


1. Otwinowski Z, Minor W (1997) Processing of X-ray diffraction data collected in oscillation mode. *Methods Enzymol* 276:307–326.
2. McCoy AJ (2007) Solving structures of protein complexes by molecular replacement with Phaser. *Acta Crystallogr D Biol Crystallogr* 63(Pt 1):32–41.
3. Adams PD, et al. (2002) PHENIX: Building new software for automated crystallographic structure determination. *Acta Crystallogr D Biol Crystallogr* 58(Pt 11):1948–1954.
4. Emsley P, Cowtan K (2004) Coot: Model-building tools for molecular graphics. *Acta Crystallogr D Biol Crystallogr* 60(Pt 12 Pt 1):2126–2132.
5. Laskowski RA, MacArthur MW, Moss DS, Thornton JM (1993) PROCHECK: A program to check the stereochemical quality of protein structures. *J Appl Cryst* 26:283–291.
6. DeLano WL (2002) *Pymol Molecular Graphics System* (DeLano Scientific, San Carlos, CA).
7. Liu DG, et al. (2009) A dedicated small-angle X-ray scattering beamline with a superconducting wiggler source at the NSRRC. *J Synchrotron Radiat* 16(Pt 1):97–104.
8. Hura GL, et al. (2009) Robust, high-throughput solution structural analyses by small angle X-ray scattering (SAXS). *Nat Methods* 6(8):606–612.
9. Guinier A (1955) *Small Angel Scattering of X-Rays* (Wiley Interscience, New York).
10. Svergun DI (1992) Determination of the regularization parameter in indirect-transform methods using perceptual criteria. *J Appl Cryst* 25:495–503.
11. Yang Z, et al. (2012) UCSF Chimera, MODELLER, and IMP: An integrated modeling system. *J Struct Biol* 179(3):269–278.
12. Pelikan M, Hura GL, Hammel M (2009) Structure and flexibility within proteins as identified through small angle X-ray scattering. *Gen Physiol Biophys* 28(2):174–189.
13. Schneidman-Duhovny D, Hammel M, Sali A (2010) FoXS: A web server for rapid computation and fitting of SAXS profiles. *Nucleic Acids Res* 38(Web Server issue): W540–W544.


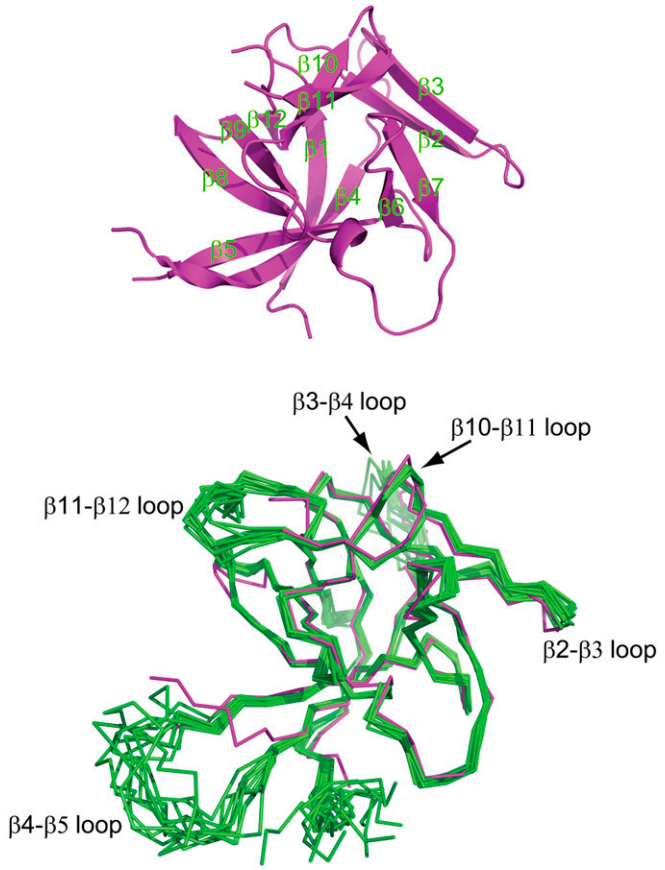


**Fig. S1.** Comparison of IL-33 structure determined by X-ray crystallography and NMR methods. (*Upper*) Cartoon diagram of IL-33 crystal structure with 12 β-stands labeled. (*Lower*) The superimposition of IL-33 crystal structure (purple) from the IL-33–ST2 complex, with 10 ensembles of IL-33 solution structure (green) determined by NMR method.

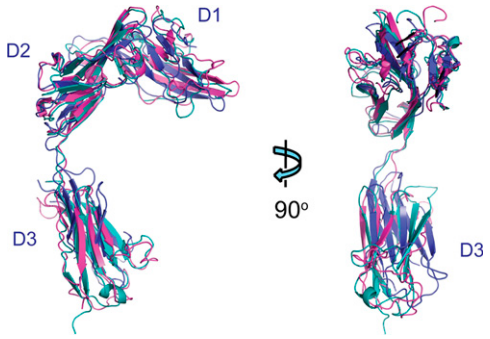


**Fig. S2.** Structural comparison of ST2 (blue) with IL-1RI (cyan) and IL-1RII (purple).

A

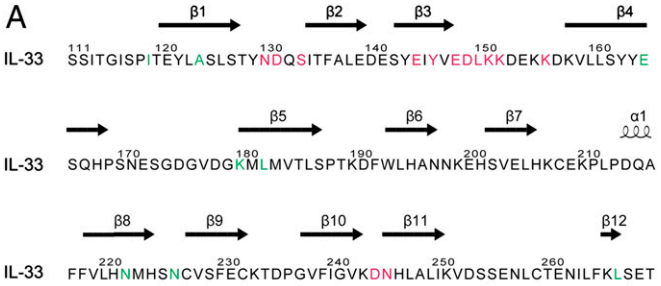


B

| IL-33 | ST2 |
|---|---|
| Ile119 | Lys257 |
| Ala124 | Phe245 |
| Asn130 | Tyr132 |
| Asp131 | Tyr119, Tyr132 |
| Ser133 | Tyr119 |
| Glu144 | Arg38, Gln39 |
| Tyr146 | Pro37 |
| Glu148 | Lys22 |
| Asp149 | Tyr119, Thr135 |
| Leu150 | Tyr119 |
| Lys151 | Met118 |
| Lys152 | Asp115, Met118, Tyr119 |
| Lys156 | Tyr119 |
| Glu165 | Leu311, Arg313 |
| Lys180 | Leu311 |
| Leu182 | Asn307 |
| Asn222 | Leu308, His309 |
| Asn226 | Phe245 |
| Asp244 | Arg35 |
| Asn245 | Arg35, Asp137 |
| Leu268 | Phe245 |

Residues at Site 1

Residues at Site 2

**Fig. S3.** Residues involved in the binding of IL-33 with ST2. (*A*) Primary sequence of IL-33 in which 12 β-strands are marked with arrows. IL-33 residues at binding sites 1 and 2 are colored with red and green, respectively. (*B*) Contacting residues at the IL-33/ST2 binding interface ($d \leq 3.5$ Å).

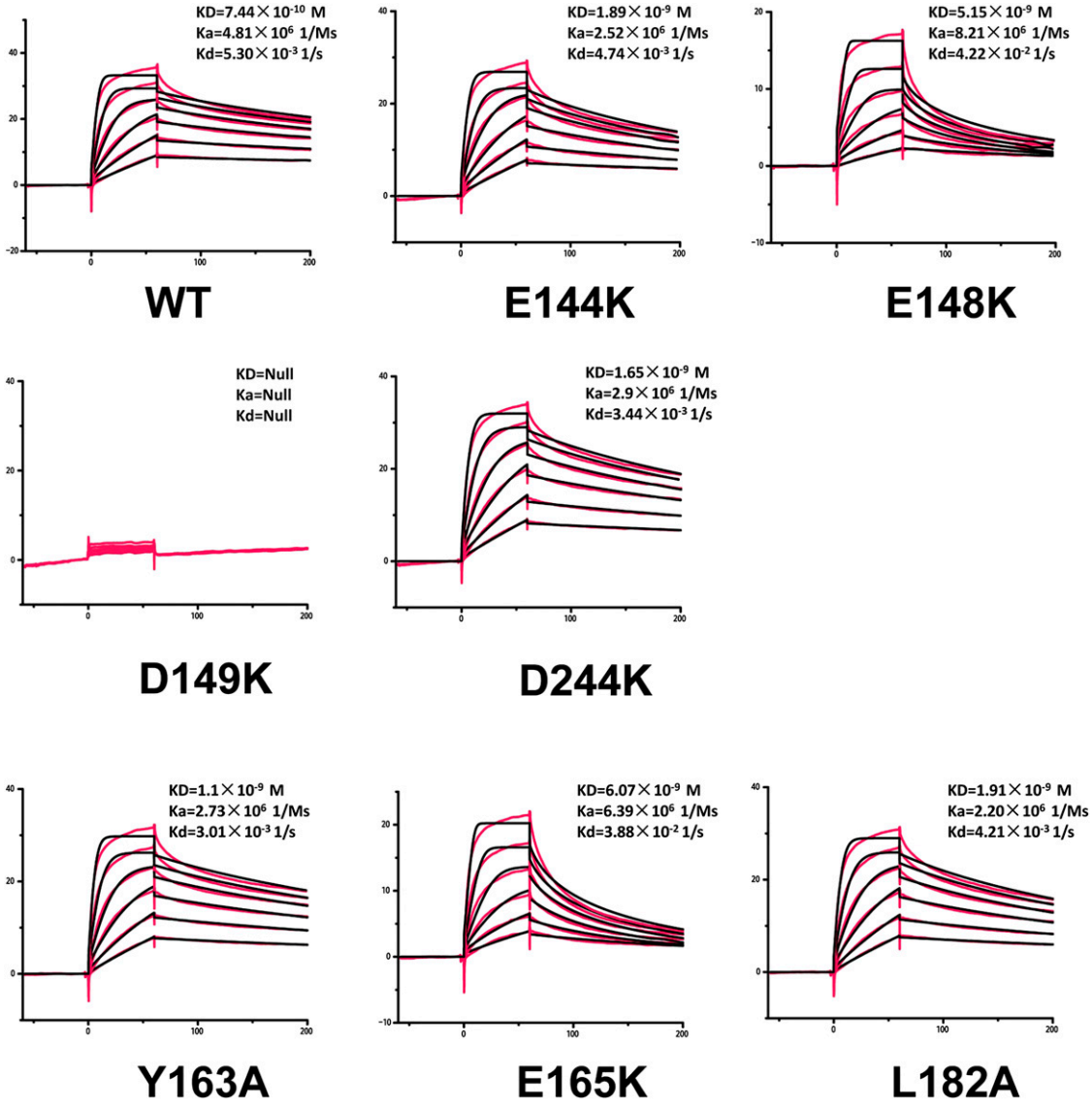


**Fig. S4.** SPR sensorgrams for the binding of IL-33 wild-type (WT) and mutants with ST2.

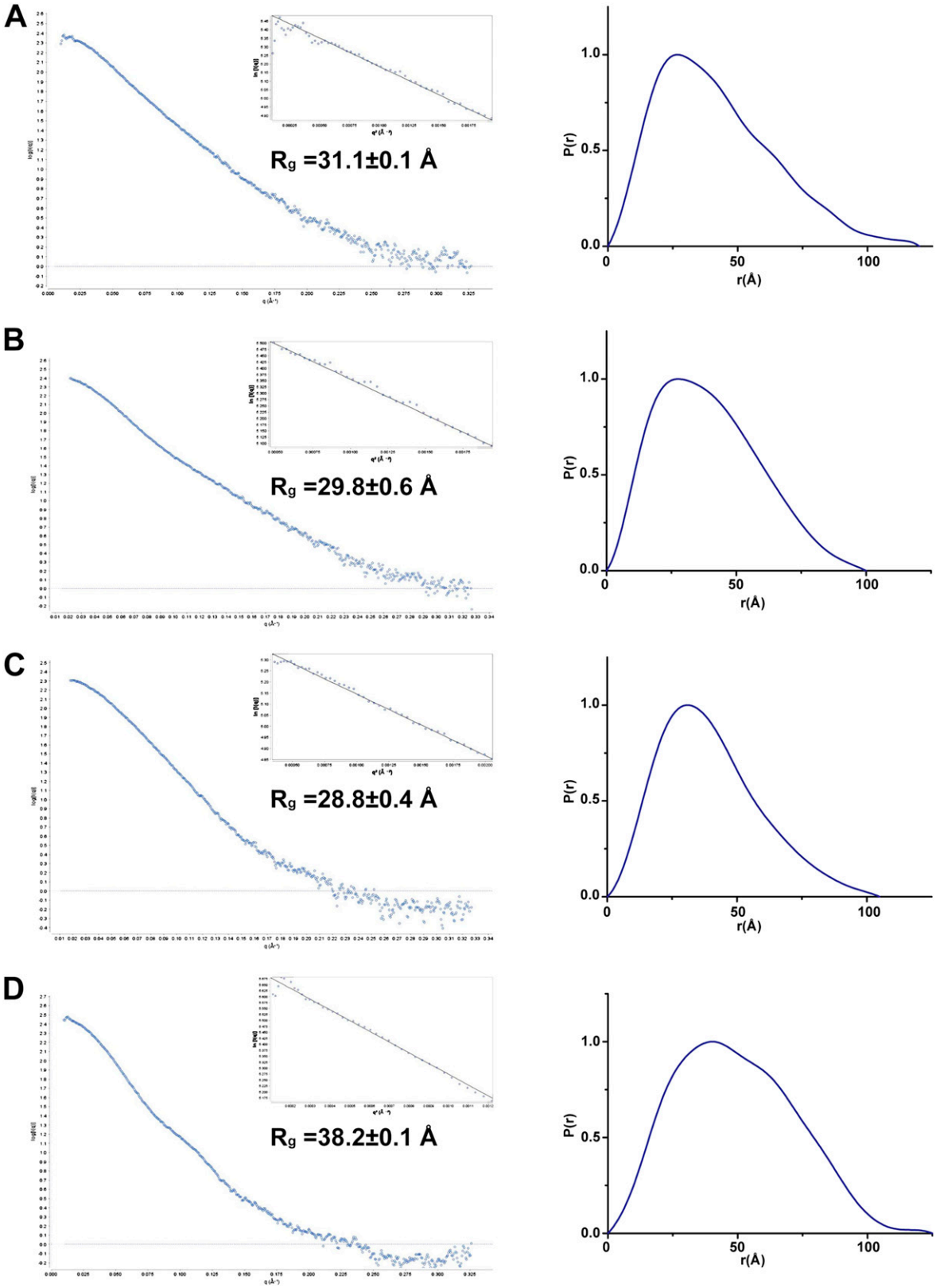


**Fig. S5.** SAXS data. Experimental scattering profiles and P(r) functions of ST2 (*A*), IL-1RAcP (*B*), IL-33–ST2 complex (*C*), and IL-33–ST2–IL-1RAcP complex (*D*). *Insets* show the Guinier plot with linear fit and the corresponding radius of gyration ($R_g$) values. P(r) functions are normalized to unity at their maxima. The maximal distance estimated from P(r) function calculated by GNOME is ∼120 Å for ST2, ∼100 Å for IL-1RAcP, ∼105 Å for IL-33–ST2, and ∼125 Å for IL-33–ST2–IL-1-RAcP.

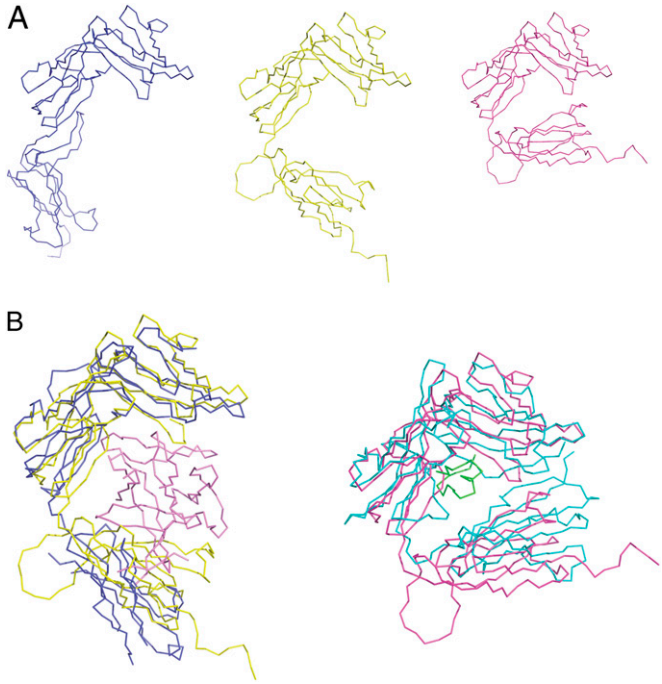


**Fig. S6.** ST2 conformers revealed by SAXS studies. (*A*) Three conformers of free ST2 in solution can be regarded as in open (blue), half-open (yellow), and closed (purple) states. (*B*) (*Left*) The superimposition of free ST2 in half-open state (yellow) with the complex of IL-33 (violet) with ST2 (blue). (*Right*) The superimposition of free ST2 in closed state (magenta) with the complex of IL-1RI (cyan) with a peptide antagonist (green) (PDB ID code 1G0Y) (1). When IL-1RI binds to the peptide antagonist, the D3 domain not only moves very close to the D1D2 module but also rotates ~170° relative to its position in the complex with IL-1β (1). In this closed state of ST2, the D3 domain just moves close to the D1D2 module without self-rotation.

1. Vigers GP, Dripps DJ, Edwards CK, 3rd, Brandhuber BJ (2000) X-ray crystal structure of a small antagonist peptide bound to interleukin-1 receptor type 1. *J Biol Chem* 275(47):36927–36933.

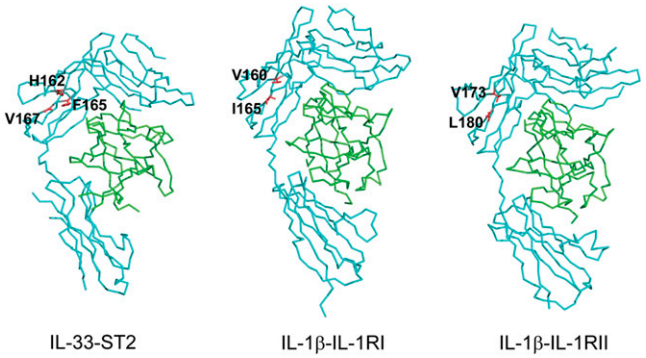


**Fig. S7.** Small conserved hydrophobic patch in IL-1 primary receptor involved in binding to IL-1RAcP.

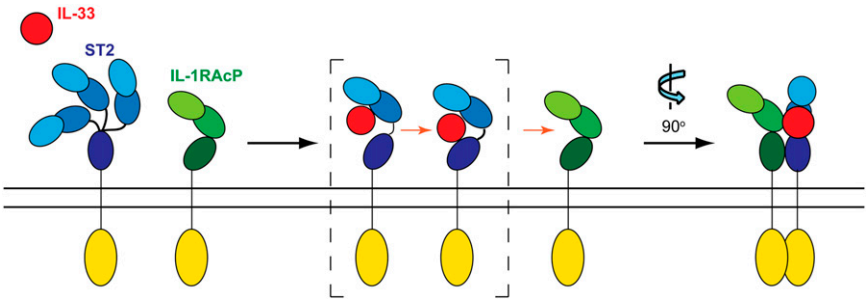


**Fig. S8.** Cartoon model of the assembly and activation of IL-33 with its receptors. IL-33 is shown in red, and the ectodomains of ST2 and IL-1RAcP are shown in blue and green, respectively. In the final 1:1:1 signaling complex, the two cytoplasmic toll/interleukin-1 receptor (TIR) domains (yellow) are proximal, resulting in activation of the intracellular signaling pathways.

**Table S1. Crystallographic data collection and refinement statistics**

| | |
|---|---|
| Data collection | |
| Beamline | SSRF BL17U |
| Wavelength | 0.9796 Å |
| Space group | H32 |
| Cell dimensions | |
| *a*, *b*, *c*; Å | 329.9, 329.9, 43.7 |
| α, β, γ; ° | 90, 90, 120 |
| Resolution, Å | 50–3.27 (3.36–3.27) |
| $R_{merge}$, % | 10.0 (72.0) |
| $I/\sigma I$ | 18.3 (2.9) |
| Completeness, % | 99.7 (100.0) |
| Redundancy | 6.0 (6.0) |
| Refinement | |
| Resolution, Å | 32.0–3.27 |
| No. of reflections | 14,000 |
| $R_{work}/R_{free}$, % | 23.8/28.7 |
| No. of atoms | |
| Protein | 3,312 |
| Glycan | 42 |
| B-factors, Å$^2$ | |
| Protein | 133.5 |
| Glycan | 110.0 |
| r.m.s. deviations | |
| Bond lengths, Å | 0.011 |
| Bond angles, ° | 1.695 |
| Ramachandran plot | |
| Most favored | 86.9 |
| Additional allowed | 10.9 |
| Generously allowed | 2.2 |
| Disallowed | 0.0 |

**Table S2. Kinetic analyses of IL-33 (WT and mutants) interacting with ST2 by SPR**

| Position | Sample | Concentration (twofold dilution), nM | $k_a$, 1/ms | $k_d$, 1/s | $K_D$, M |
|---|---|---|---|---|---|
| | WT | 3.9–125 | $4.81 \times 10^6$ | $5.30 \times 10^{-3}$ | $7.44 \times 10^{-10}$ |
| Site 1 | E144K | 3.9–125 | $2.52 \times 10^6$ | $4.75 \times 10^{-3}$ | $1.89 \times 10^{-9}$ |
| | E148K | 3.9–125 | $8.21 \times 10^6$ | $4.22 \times 10^{-2}$ | $5.15 \times 10^{-9}$ |
| | D149K | 3.9–125 | Null | Null | Null |
| | D244K | 3.9–125 | $2.9 \times 10^6$ | $3.44 \times 10^{-3}$ | $1.65 \times 10^{-9}$ |
| Site 2 | Y163A | 3.9–125 | $2.73 \times 10^6$ | $3.01 \times 10^{-3}$ | $1.10 \times 10^{-9}$ |
| | E165K | 3.9–125 | $6.39 \times 10^6$ | $3.88 \times 10^{-2}$ | $6.07 \times 10^{-9}$ |
| | L182A | 3.9–125 | $2.20 \times 10^6$ | $4.21 \times 10^{-3}$ | $1.91 \times 10^{-9}$ |